JOURNAL OF Materials CHEMISTRY

Structural deformation and non-stoichiometry of $La_4Co_3O_{10+\delta}$

Helmer Fjellvåg,*[a] Ole H. Hansteen,[a] Bjørn C. Hauback[b] and Peter Fischer[c]

[a]*Department of Chemistry, University of Oslo, N-0315 Oslo, Norway*
[b]*Institute for Energy Technology, N-2027 Kjeller, Norway*
[c]*Laboratory for Neutron Scattering, ETHZ & PSI, CH-5232 Villigen PSI, Switzerland*

Received 22nd October 1999, Accepted 5th January 2000

The structural deformation and the incorporation of an excess of oxygen in $La_4Co_3O_{10+\delta}$ have been investigated for the compositions $\delta=0.00$ and $\delta=0.30$. Rietveld analysis of high-resolution powder neutron diffraction data reveals symmetry lowering due to the displacement of oxygen atoms from the ideal positions of the Ruddlesden–Popper type structure, space group $P2_1/a$. The resulting rotations of the CoO_6 octahedra within the triple perovskite layers are similar to that commonly found in perovskites. However, the octahedra at the interface towards the LaO layers are less tilted, but more distorted than the central octahedra of the triple perovskite layers. The additional 0.30 oxygen atom of $La_4Co_3O_{10.30}$ is distributed on interstitial, tetrahedral sites within the LaO layers (ideal coordinates ¼,¼,¾). Bond valence sum calculations show that the symmetry reduction, the structural distortions and the incorporation of additional oxygen result in relief of structural strain of $La_4Co_3O_{10+\delta}$. The strain is probably caused by size mismatch between the LaO and CoO structural fragments.

Introduction

Oxygen excessive non-stoichiometry is rather common among transition metal oxides of K_2NiF_4 type, *e.g.* for $La_2CuO_{4+\delta}$ the existence range covers $0.00\leqslant\delta\leqslant0.12$,[1,2] for $La_2NiO_{4+\delta}$ $0.00\leqslant\delta\leqslant0.25$,[3–5] for $La_2CoO_{4+\delta}$ $0.00\leqslant\delta\leqslant0.27$,[1] and similar behaviour probably also occurs for $La_2MnO_{4.15}$.[6] The crystal chemistry for some of these phases is actually very complex. Stoichiometric La_2NiO_4 has three related phases in different temperature regimes. Of these, the high temperature phase has the parent tetragonal K_2NiF_4-type structure (space group *I*4/*mmm*). On cooling, related structures with tilted NiO_6 octahedra are stabilised. The size mismatch between LaO and NiO_2 layers is considered to act as a driving force for the displacive transitions. Under oxidising conditions, distinct phases of $La_2NiO_{4+\delta}$ with $0.00<\delta\leqslant0.25$ are formed.[3,4]

A particular feature for the K_2NiF_4-type structure is the presence of two-dimensional perovskite type layers of corner sharing octahedra ($LaNiO_3$). Successive perovskite layers are separated by NaCl-like structure elements (LaO). Within these NaCl-like layers there are tetrahedral voids (corresponding to the tetrahedral voids in the ccp description of NaCl) that can accommodate interstitial oxygen atoms. Such oxygen interstitials are the dominant defects in $La_2NiO_{4+\delta}$.[4,5]

The situation outlined for $La_2NiO_{4+\delta}$ also applies for other K_2NiF_4-type oxides, and could be envisaged to be of much more general nature which includes the related Ruddlesden–Popper type oxides with general formula $A_{n+1}M_nO_{3n+1}$. We have earlier reported on the crystal structure of $La_4Co_3O_{10+\delta}$ as studied by synchrotron and conventional powder X-ray diffraction.[7] $La_4Co_3O_{10+\delta}$ exists over a quite wide homogeneity range, $0.00\leqslant\delta\leqslant0.30$. In this respect, the behaviour is quite analogous to that of $La_2NiO_{4+\delta}$, however with the notable difference that no two-phase interval(s) has been detected.

It is of high interest to obtain detailed information on the oxygen excessive non-stoichiometry in this class of materials, in particular with respect to properties like superconductivity and ionic conductivity. Here, the crystal structure and non-stoichiometry of $La_4Co_3O_{10+\delta}$ is discussed on the basis of high-resolution powder neutron diffraction (PND) data. The neutrons clearly reveal that the space group symmetry is primitive and not *C*-centered as suggested by the synchrotron X-ray diffraction study. The reason is obviously related to the strong scattering contribution from the oxygen atoms in the neutron diffraction study, and may reveal the possible tilting of the CoO_6 octahedra. Results are presented for $\delta=0.00$ and 0.30. The lowering of the crystal symmetry and the occupation of interstitial tetrahedral sites are discussed on the basis of bond valence considerations.

Experimental

The $La_4Co_3O_{10+\delta}$ samples were prepared according to the citric acid method as described in ref. 7. Phase purity was assured from conventional powder X-ray diffraction (Guinier–Hägg cameras using Si as internal standard, Cu-Kα_1 and Cr-Kα_1 radiation). Stoichiometric $La_4Co_3O_{10.00}$ was obtained by calcination at 1300 K and slow cooling under flowing nitrogen, whereas the oxidised $La_4Co_3O_{10.30}$ sample was obtained by slow cooling in air. Their oxygen contents were determined gravimetrically by subsequent oxidation in pure oxygen at 1300 K for 48 hours, whereupon the samples decomposed into stoichiometric $LaCoO_3$ and La_2O_3. Note, for different oxidised samples prepared by the same procedure small deviations in oxygen content were observed, *i.e.* $0.28\leqslant\delta\leqslant0.30$.

Powder neutron diffraction data were collected with the D2B instrument, Institut Laue Langevin, Grenoble, at 22 K for $\delta=0.00$ and 298 K for $\delta=0.30$ using a wavelength $\lambda=159.38$ pm. The GSAS program system[8] was used for the Rietveld analyses. The background was modelled as a cosine Fourier series polynomial, and the peak shape was described by a pseudo-Voigt function. During initial stages of the refinement, distance restraints for the CoO_6 octahedra were introduced. Table 1 summarises characteristic features of the data sets and the variable parameters entering the least-squares refinements. Refinements were also conducted with combined data sets from high-resolution powder neutron diffraction and synchrotron X-ray diffraction experiments. For the latter data, see the earlier publication.[7]

Table 1 Characteristic features of the powder neutron diffraction data and parameters entering the profile refinements

	$La_4Co_3O_{10.00}$	$La_4Co_3O_{10.30}$
T/K	22	298
Data range (2θ/°)	8.05–149.95	5.12–157.37
$\Delta 2\theta$/°	0.05°	0.05°
Data points	2839	3046
Reflections (*hkl*)	1644	1690
Scale factor	1	1
Zero point	1	1
Profile parameters	6	6
Unit cell dimensions	4	4
Positional parameters	48	51
Isotropic displacement factors	3	4
Background coefficients	18	15
Refinable parameters	81	82

Results and discussion

Crystal structure

$La_4Co_3O_{10+\delta}$ is the $n=3$ member of the Ruddlesden–Popper series of compounds $La_{n+1}Co_nO_{3n+1}$. Our previous high resolution synchrotron powder X-ray diffraction study showed the existence of minute peak splittings, which reduces the symmetry from orthorhombic *Fmmm* to monoclinic *C*2/*m*. It was, however, impossible to refine the x and y coordinates for the oxygen atoms owing to the very dominant scattering contributions from the heavy La and Co atoms.

The PND diffraction patterns reveal the presence of reflections like (0 1 10), (12$\bar{4}$), (124), (0 1 11), (21$\bar{4}$) and (214) that violate the extinction rules for a *C*-Bravais lattice and hence space group *C*2/*m*. The systematic extinctions are consistent with space group $P2_1/a$, which proved to be the most symmetric space group to give a fully adequate fit between model and diffraction data. Unit cell data are given in Table 2.

By combination of the high-resolution synchrotron radiation data, which provide proper determination of the unit cell dimensions, with the high-resolution powder neutron diffraction data, a complete refinement allowing displacement of the oxygen atoms out of their ideal coordinates was performed. Initially the octahedral tilts were modelled with rather rigid octahedra, which were constrained by means of strong distance restraints. Thereafter the restraints were completely relaxed. Parts of the observed, calculated and difference intensity profiles which show the small differences between the two compositions $\delta=0.00$ and $\delta=0.30$ are given in Fig. 1.

The crystal structure of $La_4Co_3O_{10.00}$ is shown in Fig. 2, and crystal structure data are given in Tables 3 and 4. The unit cell comprises two triple perovskite-like layers centered at $z=0$ and 0.5, respectively. The octahedral tilts are evident in these triple perovskite-like layers. The octahedral tilting is probably due to

Table 2 Crystal structure data for $La_4Co_3O_{10+\delta}$ derived from powder neutron diffraction data. Calculated standard deviations in parentheses

	$La_4Co_3O_{10.00}$	$La_4Co_3O_{10.30}$
Space group	$P2_1/a$	$P2_1/a$
a/pm	540.73(1)	541.26(1)
b/pm	547.58(1)	546.78(1)
c/pm	2776.4(1)	2781.8(1)
β/°	90.289(1)	90.231(1)
$V/10^8$ pm^3	8.2207(6)	8.2327(6)
Z	4	4
R_p (%)[a]	3.8	4.0
R_{wp} (%)[a]	5.0	5.3
R_{exp} (%)	1.9	2.4
χ^2	6.85	5.04

[a] $R_p=100(\Sigma|I_o-I_c|/\Sigma I_o)$, $R_{wp}=100(\Sigma w(I_o-I_c)^2/\Sigma w I_o^2)^{1/2}$, $R_{exp}=R_{wp}/(\chi^2)^{1/2}$ according to ref. 8.

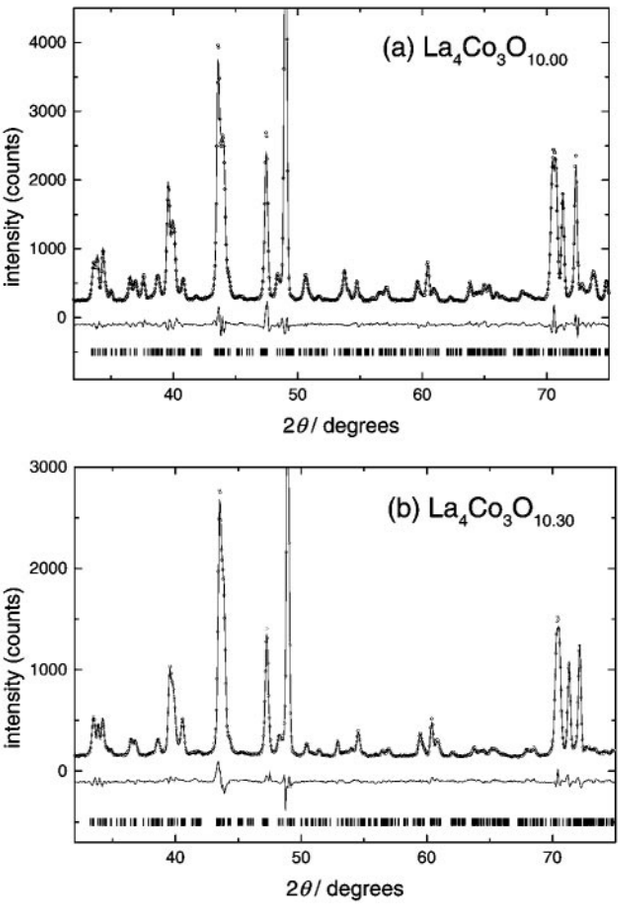

Fig. 1 Selected parts of observed, calculated and difference powder neutron diffraction profiles for (a) $La_4Co_3O_{10.00}$ and (b) $La_4Co_3O_{10.30}$, $\lambda=159.38$ pm.

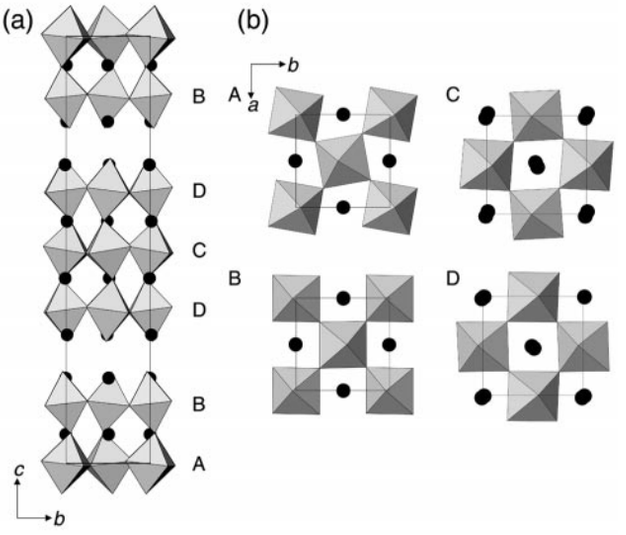

Fig. 2 Crystal structure of $La_4Co_3O_{10.00}$. (a) Projection along [100] showing the two different triple perovskite-like layers, (b) projection along [001] showing the four crystallographically different perovskite-like sheets (labelled A, B, C and D) which constitute the two triple layers. CoO_6 octahedra and La atoms (black circles) are drawn.

similar factors to those recognised for the AMO_3 perovskite type oxides,[9] *i.e.* covalency effects connected with the La atoms and minimisation of size mismatch between the La atoms occupying the twelve coordinated A sites and the voids defined by the connected network of CoO_6 octahedra. Fig. 2(b) shows projections along [001] for the four different perovskite-like

Table 3 Fractional atomic coordinates (x, y, z) for $La_4Co_3O_{10+\delta}$, $\delta=0.00$ and 0.30. Space group $P2_1/a$. Calculated standard deviations in parentheses. Isotropic displacement factors (in 10^4 pm^2): $B_{iso}(La)=0.11(3)$, $B_{iso}(Co)=0.05(1)$, $B_{iso}(O)=0.51(3)$ for $\delta=0.00$; $B_{iso}(La)=0.40(3)$, $B_{iso}(Co)=0.09(1)$, $B_{iso}(O(1–10))=0.76(4)$, $B_{iso}(O(11))=0.78(4)$ for $\delta=0.30$

	x	y	z
$\delta=0.00$			
La(1)	0.005(1)	0.012(2)	0.3012(4)
La(2)	0.494(1)	0.005(2)	0.8005(4)
La(3)	0.024(1)	0.989(1)	0.4332(3)
La(4)	0.500(1)	0.005(1)	0.9323(3)
Co(1)	0	½	½
Co(2)	0	0	0
Co(3)	0.010(3)	0.001(5)	0.139(1)
Co(4)	0.482(3)	0.011(5)	0.639(1)
O(1)	0.263(2)	0.270(2)	0.4915(5)
O(2)	0.295(2)	0.207(2)	0.9945(4)
O(3)	0.000(2)	0.052(2)	0.0714(5)
O(4)	0.505(2)	0.052(2)	0.5689(6)
O(5)	0.259(2)	0.250(3)	0.1460(5)
O(6)	0.741(2)	0.262(3)	0.6468(5)
O(7)	0.006(2)	0.960(2)	0.2150(5)
O(8)	0.491(2)	0.975(2)	0.7147(5)
O(9)	0.750(2)	0.251(3)	0.8649(6)
O(10)	0.255(2)	0.242(2)	0.3664(6)
$\delta=0.30$			
La(1)	0.002(1)	0.002(2)	0.2999(4)
La(2)	0.501(1)	0.997(2)	0.7993(4)
La(3)	0.010(1)	0.996(2)	0.4316(4)
La(4)	0.509(1)	0.001(2)	0.9328(4)
Co(1)	0	½	½
Co(2)	0	0	0
Co(3)	0.025(3)	0.998(5)	0.1345(6)
Co(4)	0.482(3)	0.995(6)	0.6426(5)
O(1)	0.288(2)	0.283(2)	0.4942(5)
O(2)	0.236(2)	0.266(3)	0.0074(5)
O(3)	0.011(2)	0.961(2)	0.0694(5)
O(4)	0.504(2)	0.053(2)	0.5670(5)
O(5)	0.252(3)	0.253(3)	0.1336(5)
O(6)	0.743(2)	0.257(3)	0.6426(6)
O(7)	0.028(2)	0.021(2)	0.2135(3)
O(8)	0.470(2)	0.940(2)	0.7103(4)
O(9)	0.741(2)	0.248(3)	0.8575(6)
O(10)	0.251(2)	0.245(3)	0.3695(5)
O(11)	0.274(6)	0.259(6)	0.746(1)

Co(1) in 2b (0,½,½); Co(2) in 2a (0,0,0); the remaining atoms in 4e (x, y, z).

sheets that constitute the two triple layers. It can be seen that the octahedral rotations around [001] are larger in the central sheets (labelled A and C) than in the top and bottom sheets of each triple layer (labelled B and D). These differences are probably due to a different coordination for the La atoms located within the triple perovskite layers, *i.e.* La(3) and La(4), than for the La atoms La(1) and La(2) located at the interface between two triple perovskite layers where a NaCl-type arrangement of La and O exists. However, from the interatomic distances given in Table 4, it is clear that the CoO_6 octahedra in the central sheets of the triple perovskite layers are quite regular, whereas those in the top and bottom sheets are considerably distorted. Such octahedral distortions will also influence the La–O coordination and the octahedral tilt.

Non-stoichiometry

The Ruddlesden–Popper type oxides have two-dimensional AO layers of NaCl-type atomic arrangement separating perovskite type blocks, $(AMO_3)_n$. In these thin layers there exist tetrahedral voids. Normally, NaCl-type oxides and halides do not accept anion interstitials owing to strong repulsion between the anions in the resulting filled Na_4Cl_4 cube. Filling of these interstices by anions would hence only be possible by substantial displacement of the anions locally. For K_2NiF_4-type oxides like $La_2NiO_{4+\delta}$ it has been shown that the differences between ideal La–O and Ni–O interatomic bond distances leads to structural strain upon intergrowth of the LaO and NiO_2 structure elements.[10] In the stoichiometric phase such structural strain is relieved by tilting of the MO_6 octahedra as described above for $La_4Co_3O_{10.00}$. This is analogous to the strain relieving mechanism of octahedral tilting in perovskites. However, for the K_2NiF_4-type oxides a further relief of the structural strain can be obtained through chemical oxidation of the transition metal atoms, thus reducing their size. For $La_2NiO_{4+\delta}$ this is achieved by incorporation of oxygen atoms in the tetrahedral interstices of the LaO layers.

When considering the location of the extra oxygen in the Ruddlesden–Popper type structure one should also recall the existence of the related series of compounds commonly known as the Auriviellius-type phases. In such phases the tetrahedral interstices of the NaCl-type layer of the Ruddlesden–Popper type structure are completely filled with oxygen atoms. Examples are $PbBi_2Nb_2O_9$ ($c=2550$ pm),[11] $Bi_4Ti_3O_{12}$ ($c=3284$ pm)[12] and $BaBi_4Ti_4O_{15}$ ($c=4160$ pm)[11] which correspond to filled Ruddlesden–Popper phases with $n=2$, 3 and 4, respectively. The general formula for such filled variants is $A_{n+1}M_nO_{3n+3}$. In order to emphasise the similarities between the Ruddlesden–Popper and Auriviellius type phases and the layered relationship to the perovskite type crystal structure, the general formulae can be rewritten as $(AO)(AMO_3)_n$ and $(AO_3)(AMO_3)_n$, respectively.

For $La_2NiO_{4+\delta}$, the maximum oxygen non-stoichiometry obtained on synthesis in air is approximately $\delta=0.18$. However, as can be seen from the schematic phase diagram based on ref. 4 in Fig. 3(a) there is no continuous non-stoichiometric $La_2NiO_{4+\delta}$ phase. On the other hand, for $La_4Co_3O_{10+\delta}$ the continuous weight increase upon cooling shown by the thermogravimetric (TGA) data in Fig. 4 indicates the existence of a wide solid solution phase with $0.00\leqslant\delta\leqslant0.30$. However, due to a too high cooling rate for the TGA experiment the data do not represent the equilibrium situation for oxidation upon cooling. Hence, the limits of the solid solution range were determined by the gravimetric analysis as described above. The schematic phase diagram in Fig. 3(b) shows that $La_4Co_3O_{10+\delta}$ similarly to $La_2NiO_{4+\delta}$ undergoes temperature-induced transitions.

A significant structural difference between $La_2NiO_{4+\delta}$ and $La_4Co_3O_{10+\delta}$ concerns the number of perovskite-like sheets in the 2-D layer. For $La_2NiO_{4.18}$ with one LaO layer for every single perovskite-like layer ($LaNiO_3$) there is 0.18 interstitial oxygen atom per LaO layer. This number is considerably larger for $La_4Co_3O_{10.30}$, which has one LaO layer per triple perovskite-like layer $(LaCoO_3)_3$, and hence 0.30 interstitial oxygen atom per LaO layer.

Comparison of the $\delta=0.00$ and $\delta=0.30$ diffraction data for $La_4Co_3O_{10+\delta}$ shows no indications for additional ordering or symmetry lowering for the latter composition. Hence, space group $P2_1/a$ was also adopted for describing the interstitial structure. Oxygen atoms were introduced into the two possible tetrahedral sites within the LaO layer (ideally ¼,¼,¼ and ¼,¼,¾). Refinement of their occupation numbers clearly showed a 100% preference for the ¼,¼,¾ site, *cf.* O(11) in Fig. 5. However, all attempts to refine the occupation number of O(11) together with the isotropic displacement factor (B_{iso}) resulted in non-physical values for B_{iso}. Hence, in the subsequent refinements the occupation of O(11) was fixed to the chemically determined oxygen content $\delta=0.30(1)$. Owing to the large number of non-equivalent atoms, $B_{iso}(Co)$, $B_{iso}(La)$ and $B_{iso}(O(1)–O(10))$ were constrained, see Table 3. Finally, the atomic coordinates for O(11) were refined, giving a certain displacement from the ideal values. Atomic coordinates and displacement factors are listed in Table 3, interatomic distances

Table 4 Selected interatomic distances (pm) and bond angles (°) for $\delta = 0.00$ and 0.30. Calculated standard deviations in parentheses. For the interstitial oxygen atom, O(11), see also text

	$\delta = 0.00$	$\delta = 0.30$
Co(1)–O(1)	2 × 192(1)	2 × 194(1)
–O(1)	2 × 197(1)	2 × 196(1)
–O(4)	2 × 193(2)	2 × 188(2)
Co(2)–O(2)	2 × 196(1)	2 × 194(1)
–O(2)	2 × 197(1)	2 × 194(1)
–O(3)	2 × 200(2)	2 × 194(2)
Co(3)–O(3)	190(3)	182(2)
–O(5)	192(3)	184(3)
–O(5)	193(3)	203(3)
–O(7)	212(3)	220(2)
–O(9)	197(3)	198(3)
–O(9)	190(3)	187(3)
Co(4)–O(4)	196(3)	214(2)
–O(6)	198(3)	200(3)
–O(6)	182(2)	187(3)
–O(8)	212(3)	191(2)
–O(10)	195(3)	186(3)
–O(10)	199(3)	200(3)
La(1)–O	240, 241, 249, 257, 258, 263, 272, 276, 298(2)	241, 241, 249, 253, 259, 269, 272, 289, 310(2)
La(1)–O(11)	—	222, 243(4)
La(2)–O	239, 243, 246, 253, 260, 262, 274, 275, 302(2)	249, 250, 255, 258, 263, 267, 268, 289, 289(2)
La(2)–O(11)	—	240, 246(4)
La(3)–O	240, 252, 256, 258, 264, 267, 277, 287, 291, 291, 297, 309(2)	243, 244, 258, 261, 264, 264, 278, 280, 281, 283, 304, 304(2)
La(4)–O	234, 248, 259, 266, 267, 272, 272, 283, 290, 293, 300, 306(2)	250, 251, 261, 261, 265, 270, 272, 280, 282, 288, 293, 296(2)
O(11)–O	—	211, 227, 251, 254(4)
O–Co(1)–O	88.5–91.5(5)	87.9–92.1(6)
O–Co(2)–O	87.6–92.4(5)	87.6–92.4(6)
O–Co(3)–O	88.0–92.4(9)	86.2–95.5(9)
O–Co(4)–O	86.4–95.3(9)	87.5–98.0(9)

and selected bond angles in Table 4. There are several structural features to be noted. First, due to the presence of the interstitial oxygen atoms, the tilt of the CoO_6 octahedra especially in the A and B perovskite type sheets of $La_4Co_3O_{10.30}$ are different from that in $La_4Co_3O_{10.00}$. Second, the calculated oxygen–oxygen distances for O(11) are rather short with an average value of 236 pm. However, since the O(11) site is only partially occupied the short distances can be considered to represent an average for the whole sample, whereas considerable local distortions of the crystal lattice are expected around the sites actually being occupied. In order to simulate the local distortion around the interstitial oxygen atoms the two neighbouring oxygen atoms, O(7) and O(8), were split into two partially occupied sites each. The refinement showed that one set of these sites was displaced away from the interstitial site, which indicates an increase in the oxygen–oxygen distances to an average value of 260 pm between the actually occupied interstitial sites and the neighbouring oxygen atoms.

Bond valence sum calculations

Brown has modelled various possible crystal structures for $La_2NiO_{4+\delta}$ by using the concept of bond valences.[10] The predicted structures corresponded well to those experimentally determined, including the existence of a miscibility gap. The situation described by Brown for $La_2NiO_{4+\delta}$ with a size mismatch resulting from the La–O–La and Ni–O–Ni bonding in respectively NaCl and perovskite type atomic arrangements applies fully to $La_4Co_3O_{10+\delta}$. Hence, in accordance with the method described by Brown, bond valence calculations were performed for $La_4Co_3O_{10+\delta}$ in order to quantify the strain relief due to symmetry reduction, structural distortions and incorporation of interstitial oxygen. For the purpose of comparison and consistency of the calculations, the unit cell dimensions for $La_4Co_3O_{10+\delta}$ at 298 K were taken from the

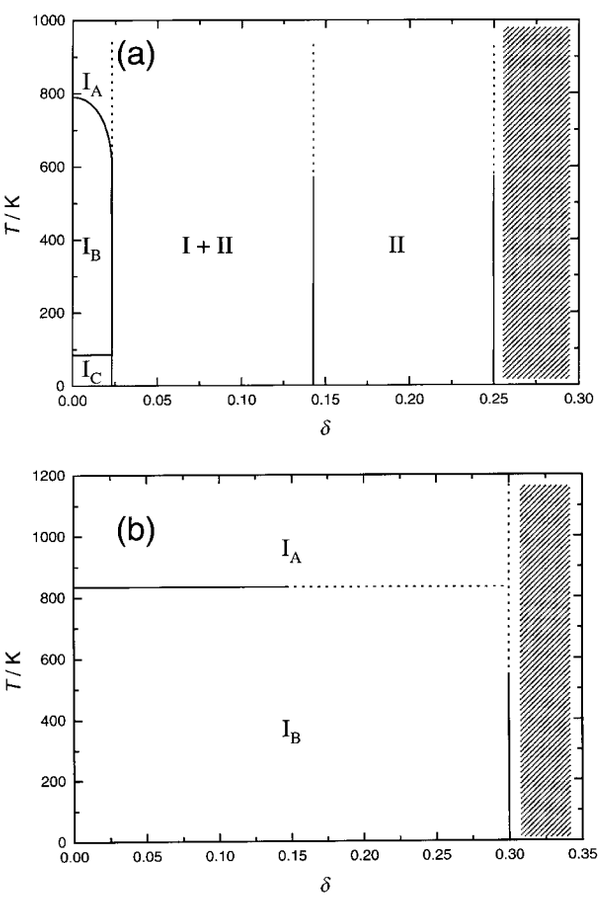

Fig. 3 Simplified phase diagrams for (a) $La_2NiO_{4+\delta}$ (based on ref. 4) and (b) $La_4Co_3O_{10+\delta}$.

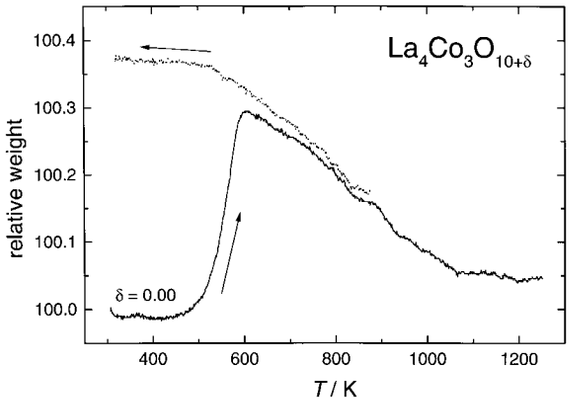

Fig. 4 TGA data showing weight change of $La_4Co_3O_{10+\delta}$ during heating and cooling in air.

previous synchrotron X-ray diffraction study.[7] Furthermore, for the mixed valence compound $La_4Co_3O_{10+\delta}$ there is no indication for charge ordering on the different Co sites. Hence, as a compromise for the calculation of bond valence sums (v_i) we used values for the bond valence parameters for cobalt (D_{Co}) averaged relative to the nominal valence state of Co. The applied bond valence parameters are taken from refs. 13 and 14. The results of the bond valence sum calculations are given in Table 5. A convenient measure for the overall agreement between the atomic valences and the bond valence sums over the whole structure is the index $R1$.[10,15] The uncertainty of $R1$ depends on the accuracy of the experimental determination of the interatomic distances and can be as large as 0.1.[15] For the present study the uncertainty of the $R1$ indices is approximately 0.02. A large $R1$ value is indicative of a strained structure. The most stable structure will have the lowest value of the $R1$ index. Judging from the $R1$ indices given in Table 5, the structural strain for $La_4Co_3O_{10.00}$ is relieved when the crystal symmetry is reduced from tetragonal (Model A) and orthorhombic (Model B) to monoclinic (Model C). A further strain relief is obtained when the atoms are allowed to move away from the ideal positions resulting in tilting of the CoO_6 octahedra and distortion of the coordination polyhedra of La (Model D, the refined structure as given in Table 3). The effect of these structural distortions is most obvious for the La atoms, which obtain essentially ideal bond valence sums. An additional minor decrease of $R1$ occurs when oxygen atoms are

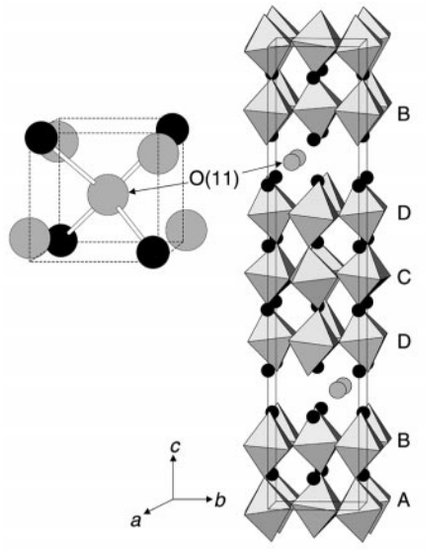

Fig. 5 Filling of interstitial tetrahedral sites in the LaO layer of $La_4Co_3O_{10.30}$. La atoms (black circles), oxygen atoms (grey circles) and CoO_6 octahedra are shown.

Table 5 Bond valence sums, v_i, for different crystal structure models of $La_4Co_3O_{10+\delta}$

	Model A $\delta=0.00$	Model B $\delta=0.00$	Model C $\delta=0.00$	Model D $\delta=0.00$	Model E $\delta=0.30$
Co(1)	3.080	3.080	3.184	3.103	3.252
Co(2)	3.028	3.028	3.045	2.832	3.131
Co(3)			3.044	3.001	3.160
Co(4)			2.956	2.959	3.009
La(1)	3.411	3.413	2.982	2.976	3.308
La(2)	2.439	2.439	2.941	2.995	2.924
La(3)			2.775	2.966	3.120
La(4)			2.683	2.987	2.932
O(1)	2.100	2.100	2.144	2.116	2.115
O(2)	1.954	1.954	2.077	2.204	2.132
O(3)	2.339	2.339	1.956	1.979	2.239
O(4)	1.686	1.688	1.985	2.156	1.971
O(5)			2.309	2.228	2.121
O(6)			2.348	2.456	2.206
O(7)			1.696	1.747	1.698
O(8)			1.699	1.741	2.058
O(9)			2.144	2.217	2.207
O(10)			2.139	2.008	2.180
O(11)					2.390
$R1$	0.33	0.33	0.26	0.23	0.21

$v_i=\Sigma\exp[D_i-d_i)/0.37]$, $D_{Co}^{II}=1.692$, $D_{Co}^{III}=1.700$, $D_{La}^{III}=2.172$,[13,14] d_i = experimentally determined interatomic distances. The used values of D_{Co} were averaged relative to the nominal valence state of Co, *i.e.* $D_{Co(\delta=0.00)}=1.6973$ and $D_{Co(\delta=0.30)}=1.6989$, see text. $R1=[(1/n)\Sigma(r_i)^2]^{1/2}$, $r_i=v_i-V_i$, *i.e.* the difference between the bond valence sum and the atomic valence of the atom, V_i. Model A: $\delta=0.00$, tetragonal unit cell, space group $I4/mmm$, $a_{Model\ A}=8^{-1/2}(a+b)_{Model\ D}$, $c_{Model\ A}=c_{Model\ D}$, Co(1) (0, 0, 0), Co2 (0, 0, 0.1392), La(1) (0, 0, 0.3013), La(2) (0, 0, 0.43314), O(1) (0, ½, 0), O(2) (0, 0, 0.0713), O(3) (0, ½, 0.1461), O(4) (0, 0, 0.2152). Model B: $\delta=0.00$, orthorhombic unit cell, space group $Fmmm$, $a_{Model\ A}=a_{Model\ D}$, $b_{Model\ A}=b_{Model\ D}$, $c_{Model\ A}=c_{Model\ D}$, Co(1) (0, 0, 0), Co2 (0, 0, 0.1392), La(1) (0, 0, 0.3013), La(2) (0, 0, 0.43314), O(1) (¼, ¼, 0), O(2) (0, 0, 0.0713), O(3) (¼, ¼, 0.1461), O(4) (0, 0, 0.2152). Model C: $\delta=0.00$. Same as Model D, but with all x and y coordinates fixed at ideal values in order to remove the tilting of the CoO_6 octahedra. Model D: $\delta=0.00$. The refined monoclinic crystal structure, space group $P2_1/a$, *cf.* Table 3 for atomic coordinates. Unit cell dimensions at 298 K are taken from ref. 7. Model E: $\delta=0.30$. Details as for Model D.

introduced into the tetrahedral positions of the LaO layers (Model E). The introduction of additional oxygen increases the atomic valence of Co, *i.e.* decreases the size of the cobalt atoms, and increases the coordination number of La. The bond valence calculations show that the three strain relieving mechanisms described by Brown for $La_2NiO_{4+\delta}$, namely symmetry lowering, atomic displacements and introduction of oxygen in interstitial positions, are also active for $La_4Co_3O_{10+\delta}$. An important difference between $La_2NiO_{4+\delta}$ and $La_4Co_3O_{10+\delta}$ is that both the octahedral rotations and the interstitial oxygen can be described by the same space group for $La_4Co_3O_{10+\delta}$. This may explain the existence of a single solid solution phase $La_4Co_3O_{10+\delta}$ over the whole composition range $0.00\leqslant\delta\leqslant0.30$.

One may envisage alternative ways to obtain oxygen excessive non-stoichiometry in Ruddlesden–Popper type phases. First, it is well known from several such systems that intergrowth of $A_{n+1}M_nO_{3n+1}$ phases with different n values may occur. The presence of such intergrowth would change the average oxygen content, and a limited extent of intergrowth would hardly be detectable by powder diffraction techniques. Second, oxygen excess non-stoichiometry is possible through the formation of cation vacancies similar to that described for perovskites like $LaMnO_{3+\delta}$.[16] Clearly, any changes in the oxygen content *via* these latter mechanisms will require large structural reorganisations of the cation sublattices by solid state diffusion. However, studies on several metastable perovskite related phases in the La–Co–O system[17,18] have

shown that such cation diffusion is kinetically hindered at those low temperatures where oxidation of $La_4Co_3O_{10.00}$ is observed (see Fig. 4; note, oxidation takes place already at 298 K in air, see ref. 7). On the other hand, bulk oxygen diffusion is easily facilitated. Hence, the interstitial oxygen mechanism discussed above is the one most probable for the incorporation of the additional oxygen atoms in $La_4Co_3O_{10.30}$. $La_2NiO_{4+\delta}$ has recently been shown to provide high oxygen ion conductivity.[19] It is probable that the conductivity is facilitated *via* the interstitial oxygen atoms, and that a similar behavior can be expected for $La_4Co_3O_{10+\delta}$.

Acknowledgements

This work has received financial support from the Research Council of Norway. The possibility of collecting data at Institut Laue Langevin, Grenoble, and the skilful assistance from the staff is gratefully acknowledged.

References

1 B. Dabrowski, J. D. Jorgensen, D. G. Hinks, Shiyou Pei, D. R. Richards, K. G. Vandervoort, G. W. Crabtree, H. B. Vanfleet and D. L. Decker, *Supercond. Appl. (Proc. Annu. Conf.), 3rd*, 1989, 379.
2 P. G. Radaelli, J. D. Jorgensen, A. J. Schultz, B. A. Hunter, J. L. Wagner, F. C. Chou and D. C. Johnston, *Phys. Rev. B*, 1993, **48**, 499.
3 H. Tamura, A. Hayashi and Y. Ueda, *Physica C*, 1996, **258**, 61.
4 J. Rodriguez-Carvajal, M. T. Fernandez-Diaz and J. L. Martinez, *J. Phys.: Condens. Matter*, 1991, **3**, 3215.
5 A. Demourgues, F. Weill, B. Darriet, A. Wattiaux, J. C. Grenier, P. Gravereau and M. Pouchard, *J. Solid State Chem.*, 1993, **106**, 317.
6 M. Lucco Borlera and F. Abbattista, *J. Less-Common Met.*, 1983, **92**, 55.
7 O. H. Hansteen and H. Fjellvåg, *J. Solid State Chem.*, 1998, **141**, 212.
8 A. C. Larson and R. B. Von Dreele, Program GSAS, General Structure Analysis System, LANSCE, MS-H 805, Los Alamos National Laboratory, Los Alamos, NM, 1998.
9 P. M. Woodward, *Acta Crystallogr., Sect. B*, 1997, **53**, 32.
10 I. D. Brown, *Z. Kristallogr.*, 1992, **199**, 255.
11 B. Aurivielliius, *Ark. Kemi*, 1949, **1**, 499.
12 E. C. Subbarro, *J. Chem. Phys.*, 1961, **34**, 695.
13 I. D. Brown and D. Altermatt, *Acta Crystallogr., Sect. B*, 1985, **41**, 244.
14 N. E. Brese and M. O'Keeffe, *Acta Crystallogr., Sect. B*, 1991, **47**, 192.
15 I. D. Brown, *Acta Crystallogr., Sect. B*, 1992, **48**, 553.
16 B. C. Tofield and W. R. Scott, *J. Solid State Chem.*, 1974, **10**, 183.
17 O. H. Hansteen, H. Fjellvåg and B. C. Hauback, *J. Mater. Chem.*, 1998, **8**, 2081.
18 O. H. Hansteen, H. Fjellvåg and B. C. Hauback, *J. Mater. Chem.*, 1998, **8**, 2089.
19 V. V. Vashook, I. I. Yushkevich, L. V. Kokhanovsky, L. V. Makhnach, S. P. Tolochko, I. F. Kononyuk, H. Ullmann and H. Altenburg, *Solid State Ionics*, 1999, **119**, 23.

Paper a908432k